Adsorption (2013) 19:1273–1290
DOI 10.1007/s10450-013-9569-5

# On the hysteresis loop and equilibrium transition in slit-shaped ink-bottle pores

**Nikom Klomkliang · D. D. Do · D. Nicholson**

Received: 8 April 2013 / Accepted: 14 August 2013 / Published online: 28 August 2013


**Abstract** Bin grand canonical Monte Carlo simulations have been carried out to study adsorption–desorption of argon at 87.3 K in a model ink-bottle mesoporous solid in order to investigate the interplay between the pore blocking process, controlled by the evaporation through the pore mouth via the meniscus separating the adsorbate and the bulk gas surroundings, and the cavitation process, governed by the instability of the stretched fluid (with a decrease in pressure) in the cavity. The evaporation mechanism switches from pore blocking to cavitation when the size of the pore neck is decreased, and is relatively insensitive to the neck length under conditions where cavitation is the controlling mechanism. We have applied the recently-developed Mid-Density scheme to determine the equilibrium branch of the hysteresis loop, and have found that, unlike ideal simple pores of constant size and infinite length, where the equilibrium transition is vertical, the equilibrium branch of an ink-bottle pore has three distinct sub-branches within the hysteresis loop. The first sub-branch is steep but continuous and is close to the desorption branch (which is typical for a pore with two open ends); this is associated with the equilibrium state in the neck. The third sub-branch is much steeper and is close to the adsorption branch (which is typical for either a pore with one end closed or a closed pore), and is associated with the equilibrium state in the cavity. The second sub-branch, connecting the other two sub-branches, has a more gradual slope. The domains of these three sub-branches depend on the relative sizes of the cavity and the neck, and their respective lengths. Our investigation of the effects of changing neck length clearly demonstrates that cavitation depends, not only on fluid properties, as frequently stated, but also on pore geometry.

**Keywords** Adsorption · Ink-bottle pores · Hysteresis · Pore blocking · Cavitation · Equilibrium transition

N. Klomkliang · D. D. Do (✉) · D. Nicholson
School of Chemical Engineering, University of Queensland, St. Lucia, Brisbane, QLD 4072, Australia
e-mail: d.d.do@uq.edu.au

N. Klomkliang
School of Chemical Engineering, Suranaree University of Technology, Nakhon Ratchasima 30000, Thailand

## 1 Introduction

The bottle shaped model holds a special place in discussions of adsorption in porous materials. The model was first proposed by McBain (1935) (who originated the term ink-bottle) as a possible explanation for the existence of hysteresis in the adsorption desorption isotherm. In McBain's theory, filling continued after adsorbate had condensed in the narrow neck because adsorbate liquid was driven into the pore by increasing pressure (Sing et al. 1985). As pressure was lowered again through the desorption branch, the wide body remained filled, even after it became sub-critical, because it was trapped by supercritical adsorbate in the narrow neck. Later studies elaborated this idea into a network model where adsorbate in wide sections remained trapped until a percolation path opened up through narrower pore sections (Nicholson 1968; Mason 1983; Liu et al. 1993; Mayagoitia et al. 1997). Subsequent detailed studies of adsorption and desorption in model pores (Nguyen et al. 2011; Ravikovitch and Neimark 2002; Grosman and Ortega 2008, 2011; Vishnyakov and Neimark 2001, 2003a, 2003b; Libby and Monson 2004; Rasmussen et al. 2012; Neimark et al. 2003; Puibasset 2010; Jorge and

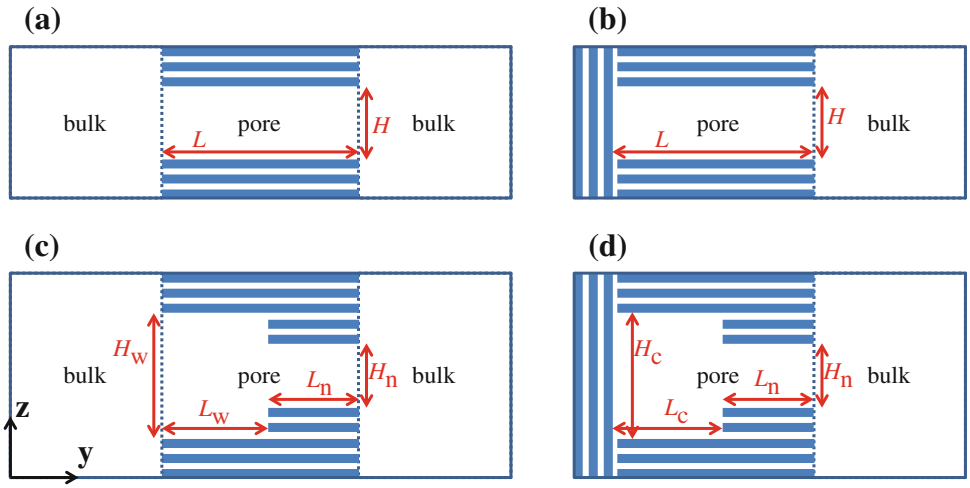


**Fig. 1** Schematic diagrams of slit-shaped pores with finite length in the *y*-direction. A periodic boundary condition was applied in the *x*-direction. (**a**) finite simple slit pore; (**b**) finite slit pore with one closed end; (**c**) two connected pores exposed to bulk; (**d**) ink-bottle pore (one cavity with one neck)

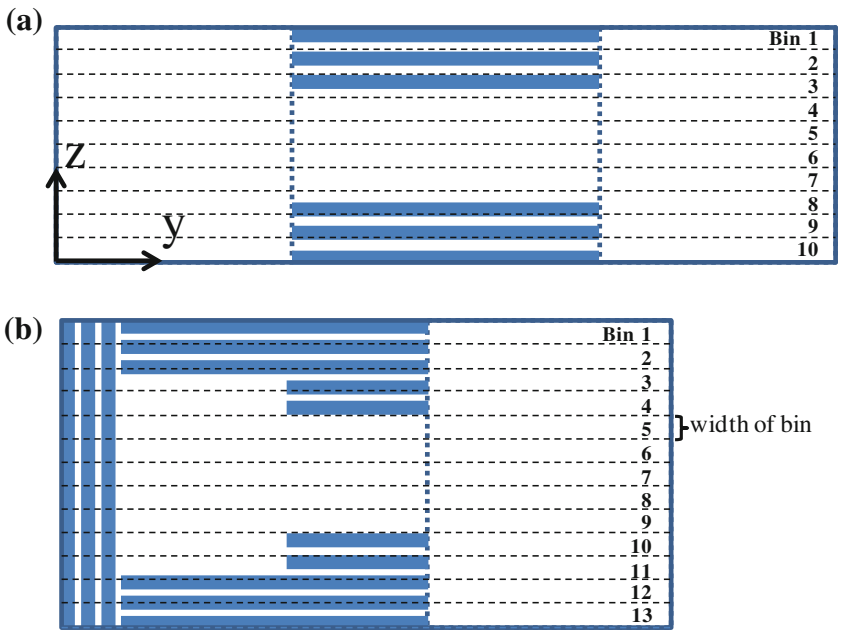


**Fig. 2** Examples of bins in a simulation box: (**a**) a simple slit-pore; (**b**) an ink-bottle pore. The number of bins depends on the width of simulation box; the bins are of approximately 0.2 nm width

Seaton 2002) have shown that the mechanism of filling and emptying is more complicated. Although trapping of the kind proposed by McBain can occur, pore structures of this general type may also empty before the trapping section becomes subcritical through a cavitation mechanism. Nevertheless, the possibility remains that dead ended pores of the ink-bottle type can be present in real materials, and that interconnected wide and narrow sections are very likely to form part of an extended porous structure.

Hysteresis associated with capillary condensation and evaporation in porous materials has been the subject of immense interest over 100 years (Horikawa et al. 2011); especially the search for the controlling mechanism and its dependence on pore topology, the pore structural parameters (such as pore width and length), temperature and adsorbate. Adsorption in simple mesopores (for example open ended cylindrical pores) always exhibits hysteresis when the temperature is less than the critical hysteresis temperature or pore size is greater than a critical value (Morishige and Tateishi 2003; Morishige 2008), and the characteristics of the hysteresis loop depend on the adsorbent material, including its chemical character as well as the pore size distribution, the pore shape and the connectivity (Horikawa et al. 2004; Lu and Schüth 2006; Reichenbach et al. 2011; Grant and Jaroniec 2012; Fan et al. 2011; Edison and Monson 2012; Lu and Schüth 2005; Rasmussen et al. 2010), the adsorbate and the temperature (Morishige and Tateishi 2003; Morishige 2008; Kruk and Jaroniec 2003). The existence of hysteresis can be attributed to metastable states in the adsorbed layer along the

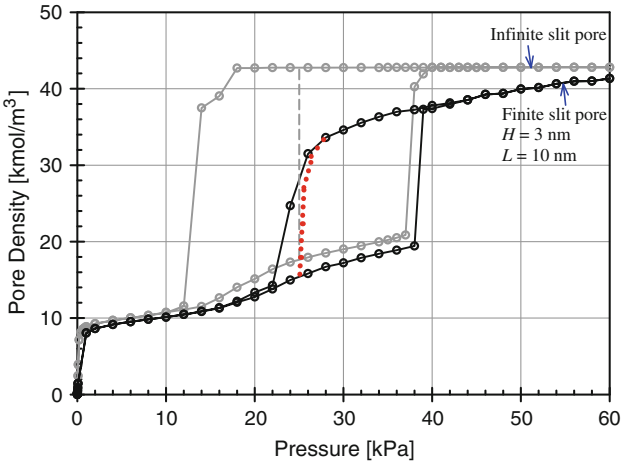


**Fig. 3** Adsorption and desorption isotherms at 87.3 K for argon in an infinite, and in a finite slit pore. The *vertical dashed line* shows the position of the equilibrium phase transition in the infinite pore. The *dotted line* shows the position of the equilibrium phase transition in the finite pore with both ends exposed to the gas reservior

adsorption branch and the metastable state of the liquid condensates along the desorption branch (Neimark and Vishnyakov 2000).

Materials such as activated carbon, porous glass and silica gel consist of interconnected networks of pores of varying shape, curvature, and size, and the experimental adsorption–desorption isotherm may exhibit single or double steps in the hysteresis loop (Ravikovitch and Neimark 2002; Grosman and Ortega 2008, 2011; Morishige and Tateishi 2003; Reichenbach et al. 2011; Lu and Schüth 2005; Rasmussen et al. 2010; Kruk and Jaroniec 2003; Rigby and Fletcher 2004; Morishige et al. 2003, 2006; Morishige and Yoshida 2010; Morishige and Yasuki 2010; Morishige and Ito 2002; Liu et al. 2008; Sahu et al. 2009). When hysteresis shows two distinct steps, the first is associated with the condensation and evaporation from the smaller pores and the second is associated with larger pores. If the pore size distribution is fairly broad, and there is no clear distinction between the distribution in the smaller and larger pores, a two-step hysteresis can become a one-step loop, as is frequently observed (Liu et al. 2008; Sahu et al. 2009). Two desorption mechanisms can be distinguished: In pore blocking, the menisci retreat from the ends of the pore, and the amount adsorbed decreases gradually as pressure is reduced, until a point at which the remaining concave lens breaks, and the amount adsorbed decreases more rapidly, giving a knee in the isotherm. The second mechanism is cavitation, where the adsorbed fluid grows a vapour-like bubble which increases in size as pressure is reduced, due to the stretching of the fluid beyond its stability limit. In some cases, it is possible for desorption to switch from pore blocking to cavitation as the temperature is increased (Morishige et al. 2006) or pressure is reduced. Pore blocking can occur in a single pore with two open ends, a single pore with one end closed, or in an ink-bottle pore with a sufficiently large neck size. Cavitation occurs mainly in ink-bottle pores that have neck sizes smaller than some critical value, and is characterized by a very steep decrease in the adsorbate density as pressure is reduced. The dominating mechanism can also depend on the adsorbate-adsorbent pair: for example, pore blocking is the mechanism of desorption for argon from porous glass at 77 K, but cavitation is the mechanism for the more weakly adsorbed nitrogen at the same temperature (Reichenbach et al. 2011). In order to explain hysteresis by either pore blocking or cavitation, a number of ink-bottle pore models have been investigated in the literature (Vishnyakov and Neimark 2003; Libby and Monson 2004; Rasmussen et al. 2012; Fan et al. 2011; Edison and Monson 2012; Sarkisov and Monson 2001; Cohan 1944).

In this study we have used computer simulation to study closed and open ended structures, constructed from slit shaped sections, in order to elucidate the details of the adsorption–desorption mechanism and in particular the path of the equilibrium transition. We have employed the recently proposed Bin Monte Carlo scheme (Fan et al. 2011) which is advantageous for studying hysteresis, because it provides better sampling than conventional Monte Carlo in dense phases, such as those encountered in desorption from a filled pore (Allen and Tildesley 1987). The method has proved to be superior to conventional MC in describing experimental observations, such as the spike in the heat curve versus loading for argon, nitrogen and methane adsorption on graphite (Fan et al. 2012). Bin-MC was previously used to study adsorption in mesopores with a uniform cross section, and it was found that the hysteresis loop is larger than that obtained by conventional MC (Fan et al. 2011), but this study was restricted to one pore size. We consider here a series of models in order to better understand cavitation induced desorption and desorption controlled by pore-blocking. The equilibrium phase transition in these pores has been determined using the Mid-Density scheme.

The Mid-Density scheme, introduced recently (Liu et al. 2011, 2012), is an alternative to more computationally demanding methods such as gauge cell Monte Carlo (Vishnyakov and Neimark 2001; 2003; Neimark et al. 2003; Puibasset 2010; Jorge and Seaton 2002; Neimark and Vishnyakov 2000), the grand thermodynamic potential (Rowley et al. 1975) or thermodynamic integration (Peterson and Gubbins 1987; Peterson et al. 1988), for locating the equilibrium transition. The method is simpler to implement and the results obtained have been shown to be in good agreement with other methods (Liu et al. 2011). Previous theoretical studies of the equilibrium phase transition in confined spaces include simulations in slit pores, cylindrical pores, and spherical pores (Vishnyakov and

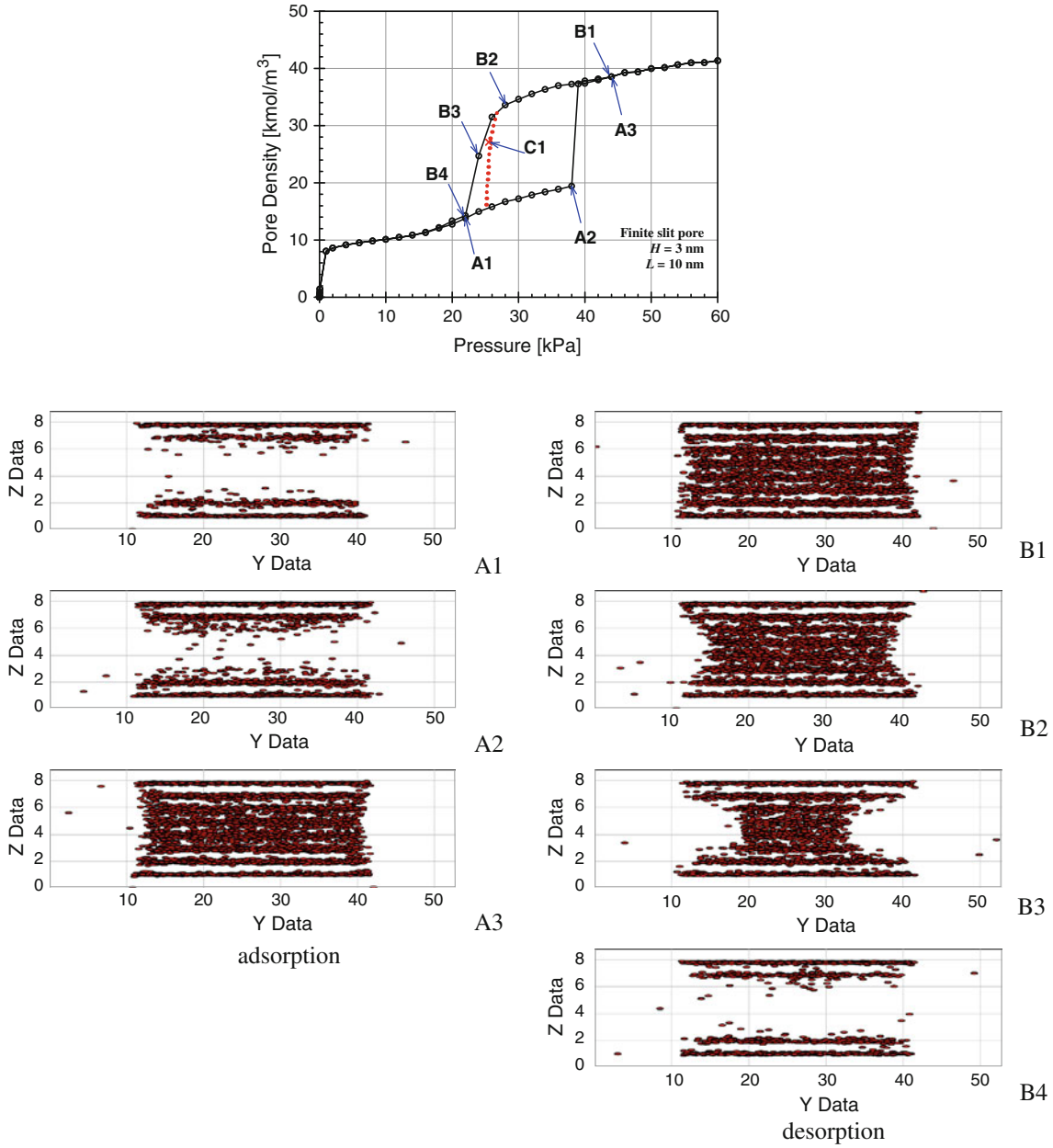


**Fig. 4** Snapshots of argon at 87.3 K along adsorption and desorption branches in a finite slit pore of width 3 nm and length 10 nm

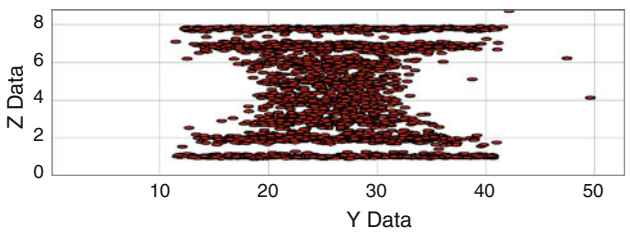


**Fig. 5** Snapshot of argon at 87.3 K at the equilibrium phase transition state (point C1 in Fig. 4) from the Mid-Density scheme in a pore of 3 nm width and length 10 nm

Neimark 2001, 2003a; 2003b; Puibasset 2010; Jorge and Seaton 2002; Neimark and Vishnyakov 2000; Liu et al. 2011, 2012; Kierlik et al. 2002), and have been restricted to pores of infinite length (via periodic boundary conditions); and a density functional study of disordered materials (Kierlik et al. 2002). It was found that the equilibrium transition in these models was first-order (Neimark et al. 2003; Jorge and Seaton 2002; Neimark and Vishnyakov 2000; Liu et al. 2011), while the transition in finite pores was found to be second order (Liu et al. 2012).

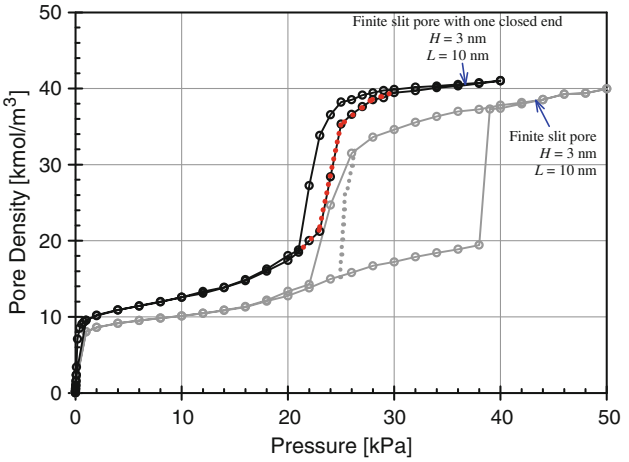


**Fig. 6** Adsorption–desorption isotherms for argon at 87.3 K in a finite slit pore (both ends are exposed to the gas reservoir) and finite slit pore with one end closed. The *dotted line* with *cross symbols* indicates the equilibrium phase transition

## 2 Theory

### 2.1 Fluid–fluid potential model

The Lennard Jones (LJ) 12–6 potential energy function has been shown to give a good description of the interaction between two argon atoms; the LJ potential parameters are $\varepsilon/kB = 119.8$ K and $\sigma = 0.3405$ nm (Hauschild and Prausnitz 1993; Do and Do 2005).

### 2.2 Fluid–solid potential model

The fluid–solid interaction energy for a slit-pore of infinite extent was calculated with the 10-4-3 Steele equation (Steele 1973). Slits of finite length in one direction were modelled as a slit pore with bulk gases at both ends as shown in Fig. 1. Four pore models were studied: (1) a pore with two open ends; (2) a pore with one end closed; (3) a pore with two connected sections of different sizes, open at the ends and (4) an ink-bottle pore connected to a gas reservoir via a neck, smaller in size than the cavity. We used the Bojan–Steele equation (Bojan and Steele 1988, 1989, 1993) to calculate the fluid–solid potential energy ("Appendix") with a spacing between the two adjacent graphite layers of 0.34 nm.

### 2.3 Bin grand canonical Monte Carlo (Bin-GCMC)

We describe the Bin-GCMC scheme (Fan et al. 2011), briefly here. The simulation box is divided into bins of 0.2 nm width along the *y*-direction, as shown in Fig. 2 for a finite pore with two open ends and for an ink-bottle pore. The simulation is carried out by selecting a bin $K$ at random and either: (1) inserting a particle at a random position in the selected bin, followed by a displacement of a randomly selected particle in that bin, or (2) deleting a randomly selected particle, followed by a displacement of a randomly selected particle. The probabilities of acceptance of a displacement move, insertion or deletion are given by Eqs. (1–3), respectively.

$$\text{Displacement: } P = \min\left\{1, \exp\left(\frac{U_{\text{new}} - U_{\text{old}}}{k_B T}\right)\right\} \tag{1}$$

$$\text{Insertion: } P = \min\left\{1, \frac{V_K}{\Lambda^3 (N_K + 1)} \exp\left[\frac{\mu - [U(N_K + 1) - U(N_K)]}{k_B T}\right]\right\} \tag{2}$$

$$\text{Deletion: } P = \min\left\{1, \frac{\Lambda^3 N_K}{V_K} \exp\left[-\frac{\mu + [U(N_K - 1) - U(N_K)]}{k_B T}\right]\right\} \tag{3}$$

where $U_{\text{new}}$ and $U_{\text{old}}$ in Eq. (1) are energies after and before the move respectively; $[U(N_K{+}1) - U(N_K)]$ in Eq. (2) is the interaction energy of the inserted particle in bin $K$ with particles of all bins and with the adsorbent; $[U(N_K{-}\ 1) - U(N_K)]$ in Eq. (3) is the interaction energy of the deleted particle with the remaining particles and adsorbent; $V_K$ and $N_K$ are volume and number of particles in bin $K$, respectively; $k_B$ is the Boltzmann constant; $T$ is the temperature; $\mu$ is the chemical potential; and $\Lambda$is the thermal de Broglie wavelength. It should be noted that the probabilities of insertion and deletion depend on the local density, rather than the overall average density used in conventional GCMC (Allen and Tildesley 1987).

In performing the simulations, the box length in the *x*- or *y*-direction was more than 10 times the collision diameter of argon, for pores of infinite length, and the cut-off radius was taken to be half of the box length. The number of configurations was $5 \times 10^7$ for both equilibration and sampling.

The average absolute and excess volumetric densities are defined by:

$$\rho_{\text{pore}}^{\text{ABS}} = \frac{\langle N \rangle}{V_{\text{acc}}}; \ \rho_{\text{pore}}^{\text{EXC}} = \frac{\langle N \rangle - \rho_{\text{b}} V_{\text{acc}}}{V_{\text{acc}}} \tag{4}$$

where $\rho_{\text{b}}$ is the bulk molecular density, $\langle N \rangle$is the ensemble average of the number of particles in the pore, and $V_{\text{acc}}$ is the accessible pore volume (Do et al. 2008).

### 2.4 Bin canonical Monte Carlo (Bin-CMC)

The system is divided into bins in the same way as in the grand canonical scheme (Fan et al. 2011). There are two

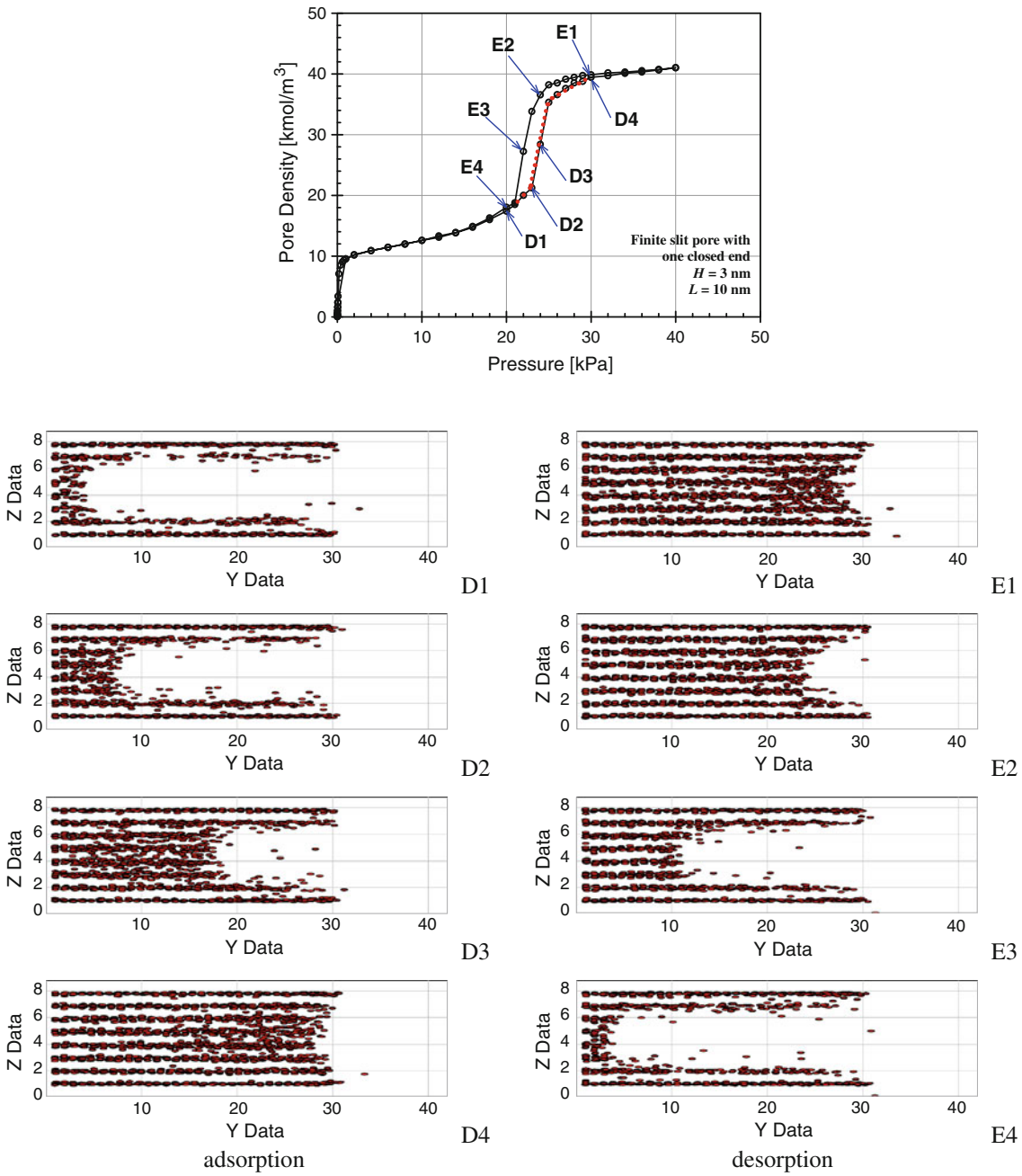


**Fig. 7** Snapshots of argon at 87.3 K along adsorption and desorption branches in a slit pore of width 3 nm and length 10 nm, with one end closed

moves: displacement, and swapping a particle between two randomly selected bins, $K$ and $L$. For the swapping move, a particle is selected at random in bin $K$ and removed, and a particle is inserted at a random position in bin $L$. After the swap, displacement moves are made in both bins, without allowing particles to cross the boundaries between bins, to ensure that microscopic reversibility is satisfied, since there are different maximum displacement lengths in each bin. The probability that a particle is deleted in bin $K$ and inserted in bin $L$ is given by Eq. (5).

$$P = \min\left\{1, \frac{(N_K/V_K)}{(N_L+1)/V_L} \exp\left(-\frac{[U(N_L+1)-U(N_L)]-[U(N_K)-U(N_K-1)]}{k_BT}\right)\right\} \quad (5)$$

## 2.5 Mid-Density scheme

The Mid-Density scheme proposed recently by Liu et al. (2011, 2012) was used here to determine the equilibrium

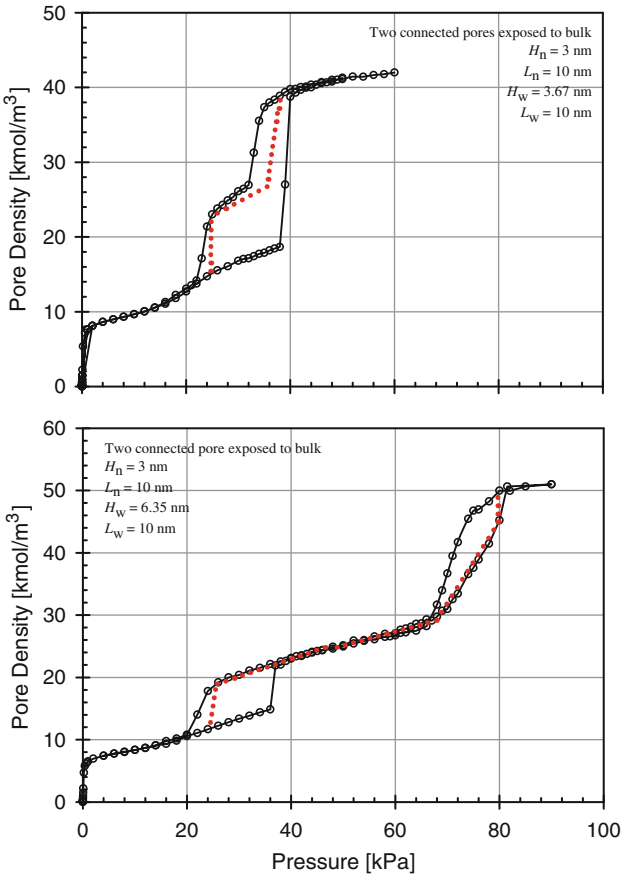


**Fig. 8** Adsorption and desorption isotherms of argon at 87.3 K in the two connected pores exposed to bulk. The dotted line is the equilibrium phase transition in the pores

phase transition. For a given chemical potential in the hysteresis loop, say $\mu^*$, the system exists in either the low density state ($\rho_L$) or the high density state ($\rho_H$), from which we calculate the arithmetic average density, $\rho_{av}$. The Mid-Density scheme starts with a canonical simulation of a system at this average density; the initial configuration can be constructed by inserting molecules in the box at the low density state until the average density is approximately achieved. Once this system has been relaxed canonically, it is then subjected to a grand canonical simulation at the chemical potential $\mu^*$; the final state from this simulation is taken to be the stable state.

## 3 Results and discussion

### 3.1 Simple slit pores

The simulated adsorption–desorption isotherms for a finite slit pore of width 3 nm and length 10 nm and for one of the same width and infinite length (i.e. periodic boundary conditions are imposed) are shown in Fig. 3.

Because the column of liquid condensate in the infinite pore evaporates less readily than that in the finite pore, the desorption pressure for the infinite pore is lower than for the finite pore, resulting in a very large hysteresis loop for the infinite pore. However, the infinite pore does does not represent experimental reality. A second difference between the infinite pore and the finite pore is that in the former the desorption branch (prior to cavitation-induced evaporation) decreases only slightly as molecules are evaporated from the end of the meniscus. In the finite pore the capacity along the desorption branch decreases much more, due a combined loss of mass at the pore mouth, from the receding menisci, and the stretching of the fluid. The menisci recede because the molecules at the gas–liquid interface are pulled towards the liquid-like region rather than towards the more rarefied region as seen in Fig. 4.

#### 3.1.1 *Equilibrium transition*

The equilibrium phase transition in an infinite slit pore is first order (shown as the vertical dashed line in Fig. 3); while the equilibrium branch for the finite length pore is steep, but continuous (second-order), and is close to the desorption branch. The reason for this proximity can be seen by comparing the snapshots at B3 in Fig. 4, and at C1 on the equilibrium branch in Fig. 5, which show that the distribution of the two phases is very similar in both cases. The snapshot in Fig. 5, for the short length pore, shows a single liquid bridge in the middle of the pore. In longer pores, two liquid bridges are formed, with a cavity in the middle, such that the interfaces between the gas-like and liquid-like regions are approximately hemi-cylindrical in shape. A similar structure was observed in our previous work (Klomkliang et al. 2013) with a 48 nm length pore.

### 3.2 Finite slit pore with one closed end

The adsorption–desorption isotherms for argon at 87.3 K in a pore of 3 nm width and length 10 nm, closed at one end, are shown in Fig. 6, together with the isotherm for an open ended pore of the same width.

The closed end of the pore has a higher adsorption affinity than the walls because of the strongly adsorbing corner sites, and adsorption follows a mechanism involving two simultaneous processes: the progression of a gas–liquid interface from the closed end towards the pore mouth, and the build up of layers on the pore wall; the former being dominant because of the greater fluid–fluid interactions resulting from the concave curvature at the gas-like side where a fluid molecule interacts with neighbouring molecules at shorter distances. As a consequence there is no sharp jump in density in the adsorption branch as there is for the open ended pore (Fig. 6). Upon

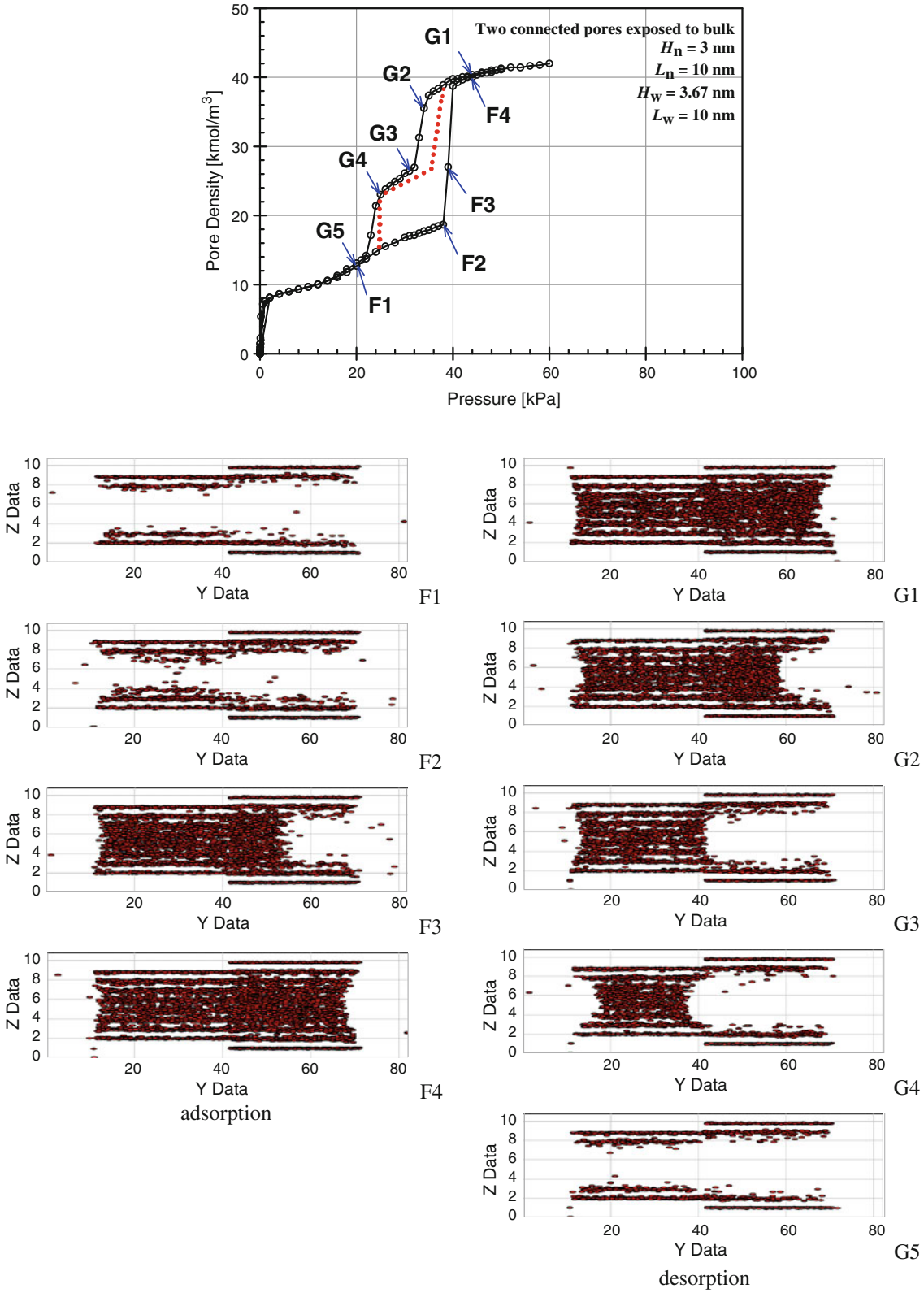


**Fig. 9** Snapshots of argon at 87.3 K along the adsorption and desorption branches from the Bin-GCMC for the two connected pores exposed to bulk

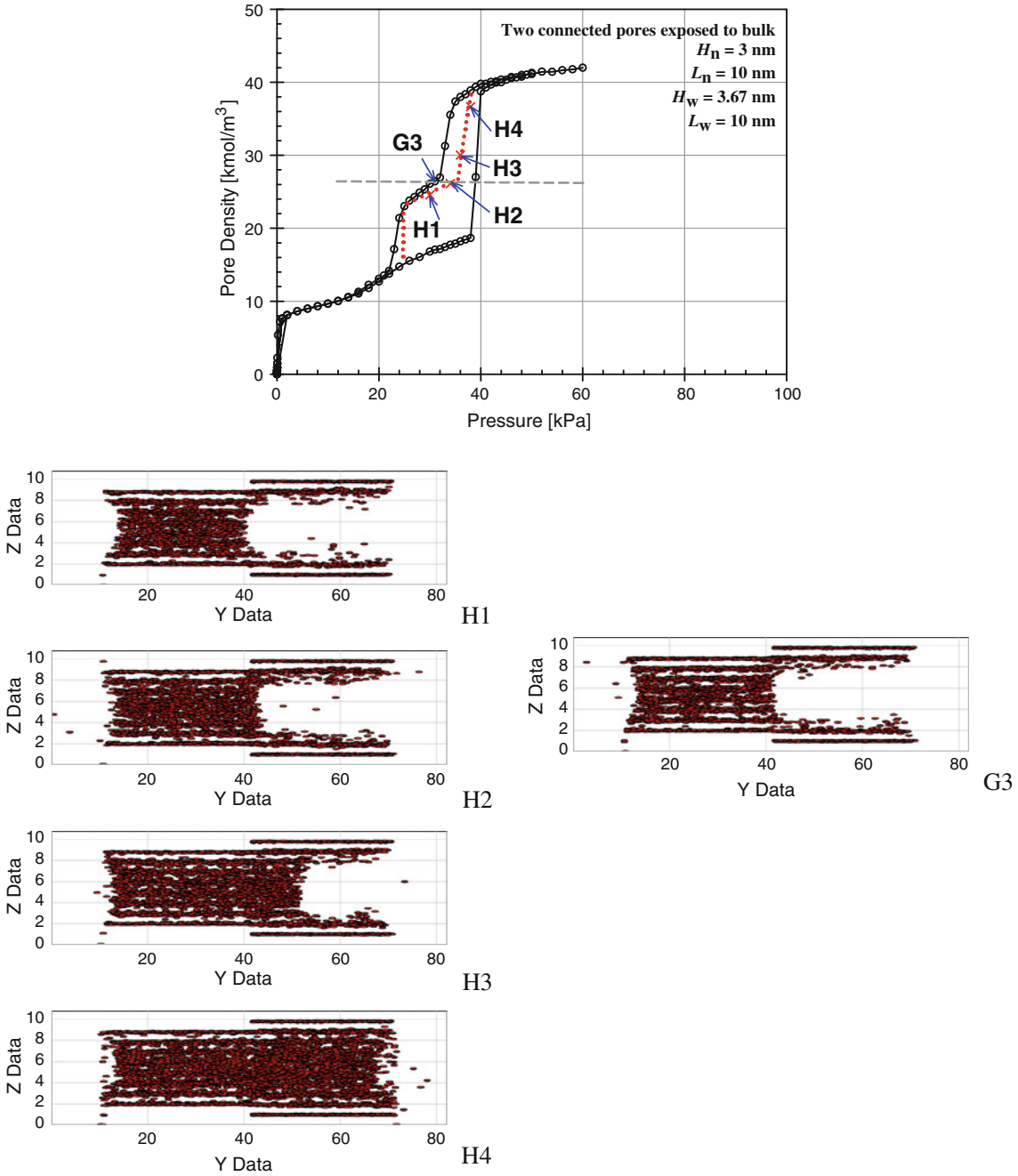


**Fig. 10** Snapshot of argon at 87.3 K for the equilibrium phase transition state from the Mid-Density scheme for the two connected pores exposed to bulk

desorption, this process is reversed, but the liquid-like region can now be maintained in a metastable state because of the cohesive force (especially at low temperatures), resulting in a hysteresis. However the loop size is much smaller than that observed for the comparable pore having two open ends. The region of metastability is less for larger pores, and therefore the loop is expected to be smaller for wider pores of the same length and for shorter pores of the same width. Snapshots for the pore of 3 nm width and length 10 nm with closed end are shown in Fig. 7. Adsorption (the left panel of the figure) starts with layering on the pore walls including the closed end, followed by the formation of a meniscus at the closed end, which progresses towards the pore mouth as pressure is increased. On desorption (the right panel) the adsorption mechanism is reversed.

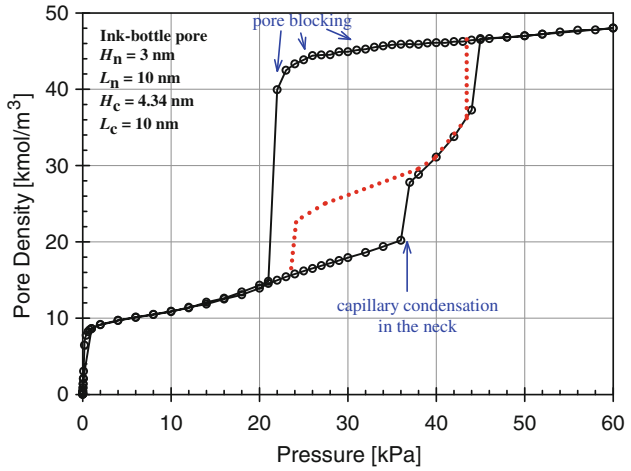


**Fig. 11** Adsorption–desorption isotherm for argon at 87.3 K in an ink-bottle pore (one closed cavity with neck). The *dotted line* shows the equilibrium phase transition

### *3.2.1 Equilibrium transition*

The equilibrium phase transition for the closed end pore is shown as a dotted line in Fig. 6, and coincides exactly with the adsorption branch of the hysteresis loop. This differs from the open ended pore, for which the equilibrium transition is closer to the desorption branch (see Fig. 3); for direct comparison we also include the results for the open ended pore in Fig. 6. There has been a lengthy debate about which branch of the hysteresis loop should be chosen for analysis of pore size distribution. From these simulations, we can tentatively conclude that equilibrium is closer to the desorption branch for open ended pores, but is much closer to the adsorption branch for pores with one closed end.

## 3.3 Two connected pores exposed to bulk

The model is shown as (c) in Fig. 1. We have selected pore widths in which hysteresis would occur if the two sections were isolated. We have chosen two examples: (1) the widths are close to each other; (2) the widths are very different. In the first case the widths of the two sections were 3 nm and 3.67 nm and the capillary condensation in this connected pore occurs in one step (the top graph of Fig. 8) because when condensation starts in the narrow section it will quickly spread to the larger section of the pore (an avalanche effect). However, upon desorption from a completely filled pore there is a two-stage desorption, because although the menisci recede from both ends of the pore, the larger end empties faster. Therefore the first stage of desorption is due to the emptying of the larger section through the larger end of the pore, and the second stage is due to the emptying of the narrow section through both ends, because the larger section is now empty except for adsorbed layers.

For the second example the widths of the two connected sections were chosen as 3 and 6.35 nm. Since the difference in sizes is very large there are two steps in the adsorption branch of the isotherm. The first step corresponds to capillary condensation in the narrower section of the pore. The larger section now behaves like a closed end pore with one end closed by the liquid condensate in the narrower section and the other end open to the surroundings (see the snapshots in Fig. 9). Adsorption in the wider section therefore progresses via movement of the meniscus towards the pore mouth at the larger end, and therefore the adsorption is gradual as seen in the bottom graph of Fig. 8. Upon desorption from the completely filled pore, there is a two-stage desorption, and the mechanism is the same as that described earlier for the first case.

### *3.3.1 Equilibrium transition*

The equilibrium phase transition is shown as the dotted line in Fig. 8. Unlike the uniform pores dealt with earlier, the equilibrium branch of a connected pore is a two-stage process. The first is second-order like (i.e. continuous rather than discontinuous), is close to the desorption branch, and is associated with the equilibrium in the narrower section of the pore. The adsorption and desorption in this narrow section behave in the same way as an independent pore with both ends open to the surrounding gas (see Sect. 3.1). The second stage is steeper, and is close to the adsorption branch of the hysteresis loop. This stage is associated with the wider section of the pore because the adsorption and desorption in this section is similar to an independent pore with one end closed, whose detailed behaviour has been discussed in Sect. 3.2.

The two stages of the equilibrium transition, which are associated with the two sections of the pore, occur over two different pressure ranges, and there exists an equilibrium branch that connects these two stages. We shall call this branch the connecting equilibrium transition. When the sizes of the two sections are not very different, this connecting equilibrium transition is between the adsorption and desorption branches of the hysteresis loop (top graph of Fig. 8). However, when the pore sizes are very different, this transition spans the desorption branch of the first hysteresis loop and the adsorption branch of the second hysteresis loop. The middle portion of this transition follows the stable states of the isotherm (bottom graph of Fig. 8).

We show, in Fig. 10, snapshots for the equilibrium phase transition for the case where the sizes of the narrow and wide sections are not very different. The snapshots of the connecting equilibrium at the points H1 and H2 show that the system evolves at the junction of the two sections. The snapshots of the equilibrium transition in the wider section of the pore (points H3 and H4) show that the

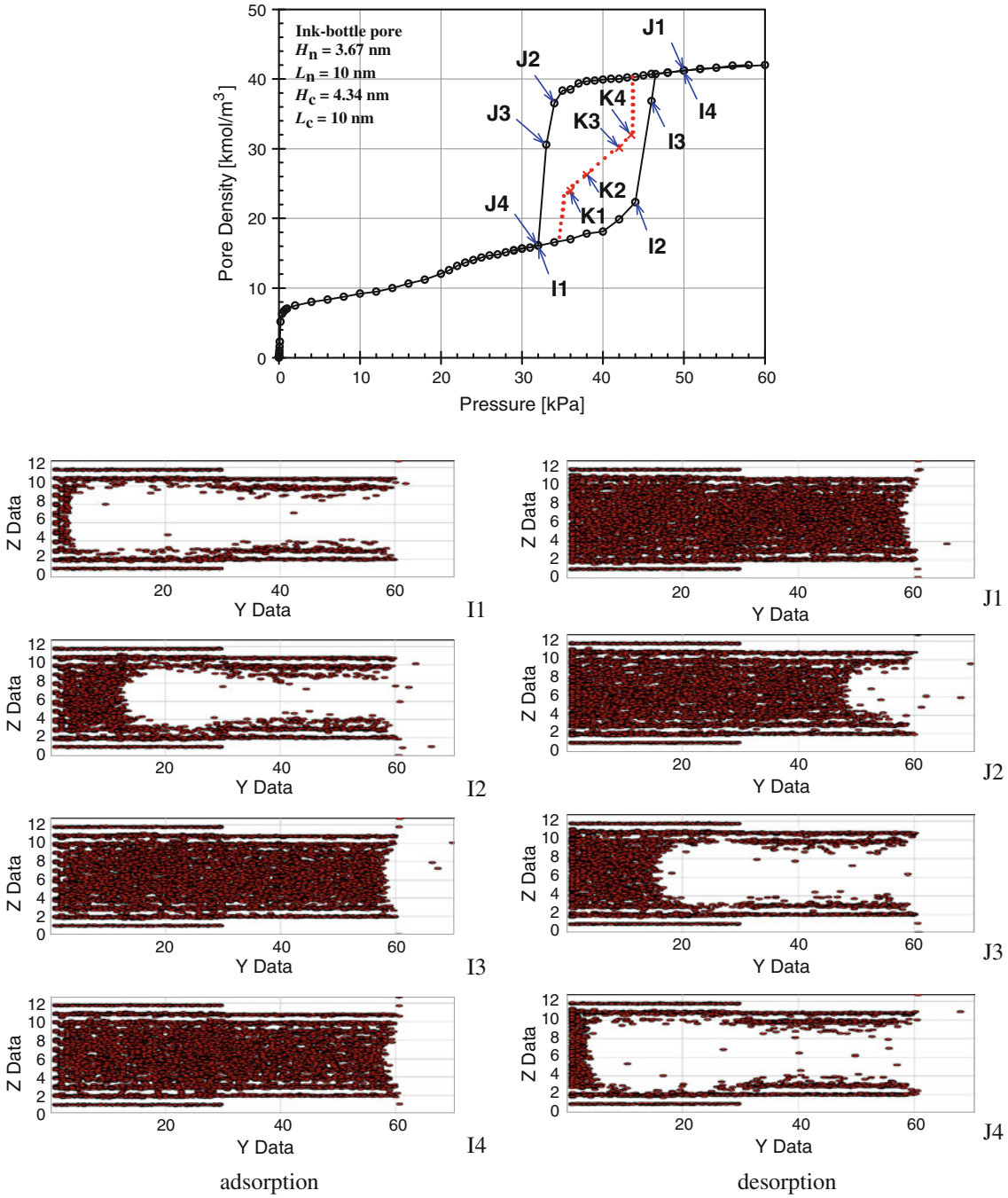


**Fig. 12** Adsorption–desorption isotherm and snapshots along the adsorption and desorption branches for argon at 87.3 K from the Bin-GCMC in an ink-bottle pore

molecules are building up a liquid bridge in the wider pore. It is interesting to study the snapshots of the metastable state (point G3) and the equilibrium transition at the same density (point H2) as shown in Fig. 10. Although the topology of these two snapshots is the same, there is a difference between these two states in the distribution of molecules in the pore.

### 3.4 Ink-bottle pore (one cavity with one neck)

We consider an ink-bottle pore where a cavity is connected to the surroundings via a neck smaller in size. The ink-bottle pore has frequently been used as the classic example for the discussion of the phenomena of cavitation and pore blocking.

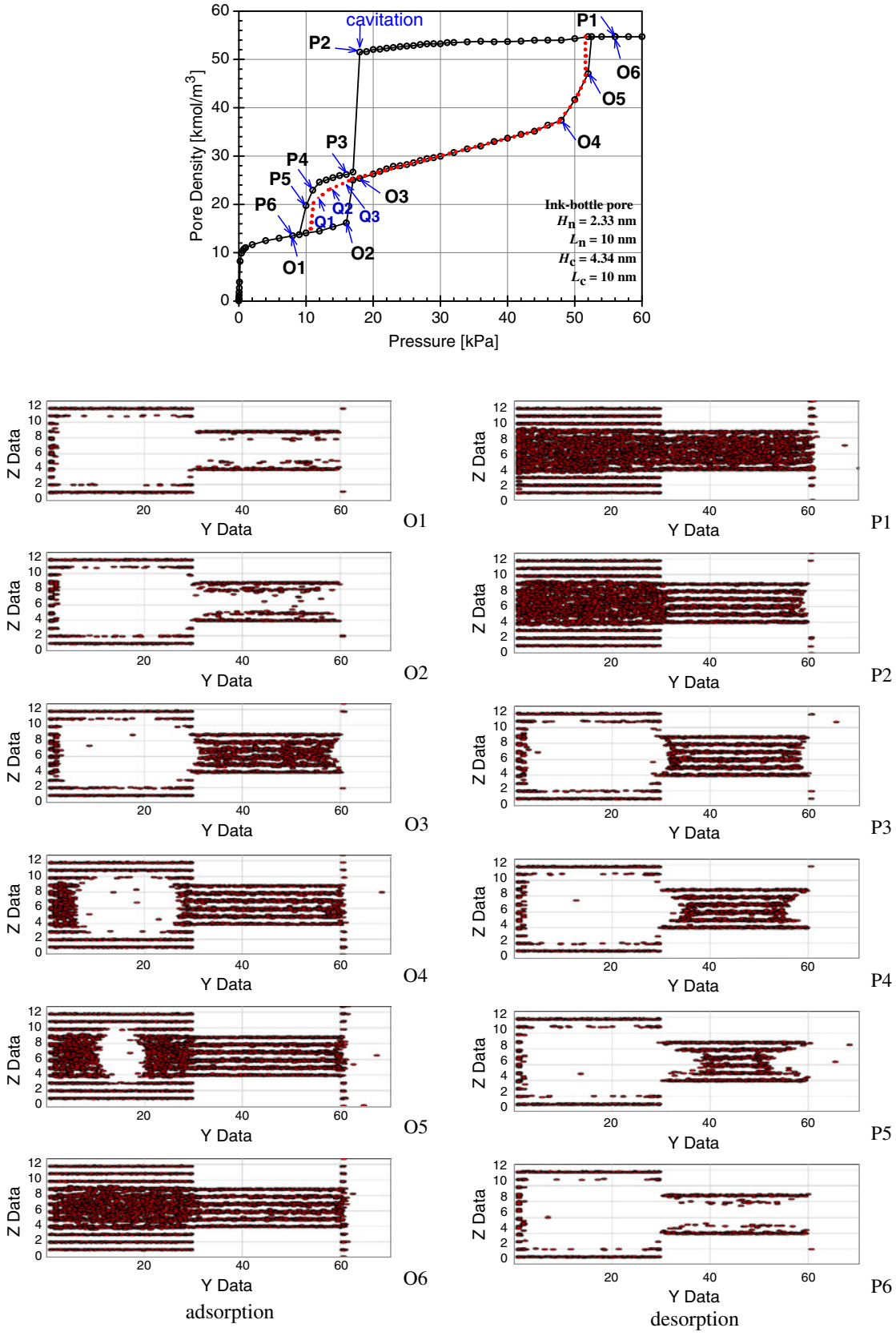


**Fig. 13** The adsorption–desorption isotherm for Ar at 87.3 K in an ink-bottle pore, and snapshots along the adsorption desorption branches showing cavitation

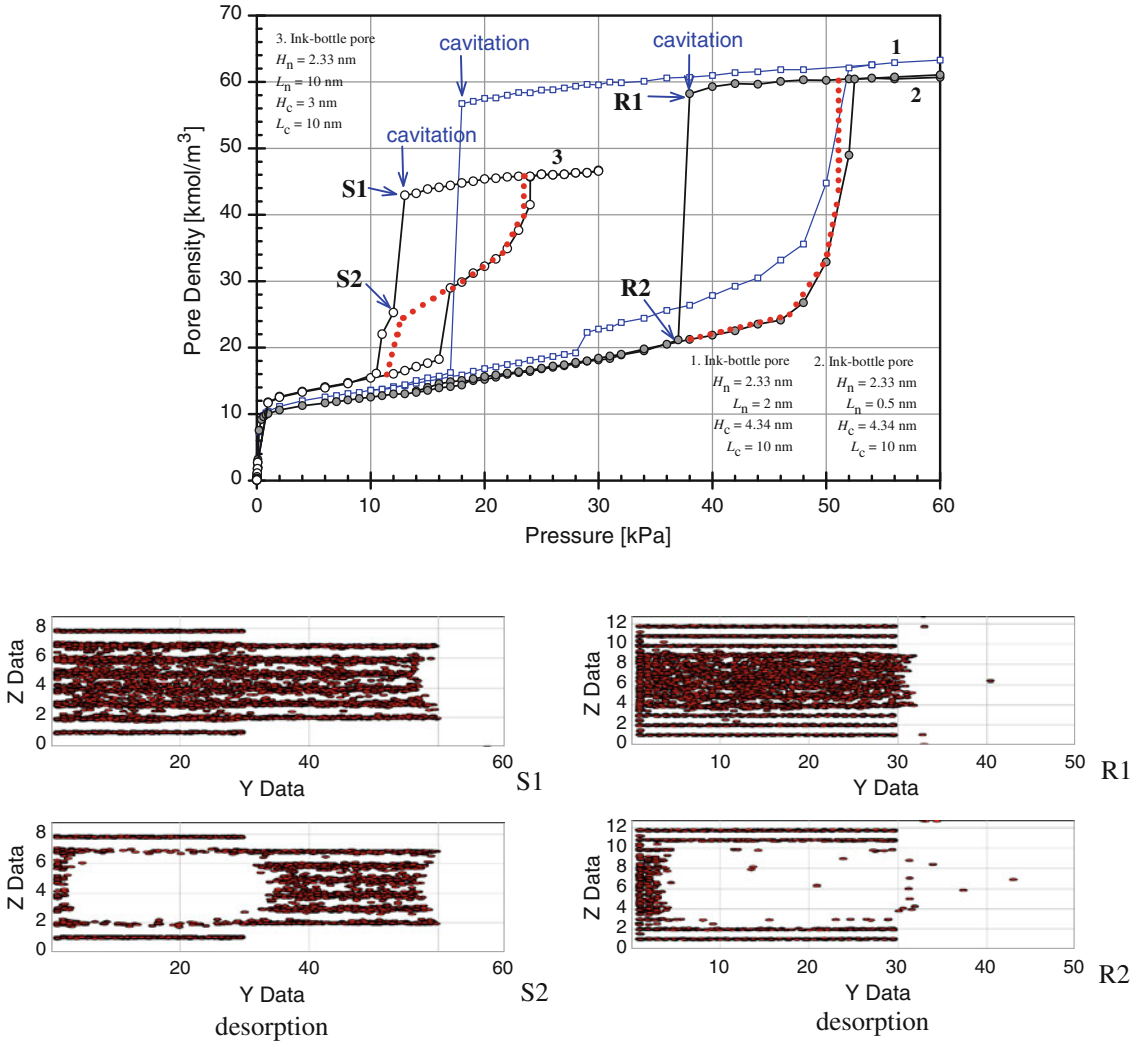


**Fig. 14** Adsorption–desorption isotherms for Ar at 87.3 K showing cavitation for pores with short and long necks, and snapshots of molecular configurations on the desorption branch. The dotted lines are the equilibrium isotherms, determined using the Mid-Density scheme

### *3.4.1 Pore blocking*

To study pore blocking, neck sizes of 3 and 3.67 nm were chosen which, for Ar at 87.3 K in this adsorbent field, are above the critical size for pore blocking, but below that for cavitation. The critical size is a function of temperature and adsorbate–adsorbent pair (Libby and Monson 2004; Rasmussen et al. 2012; Morishige and Yoshida 2010; Morishige and Yasuki 2010; Morishige and Ito 2002; Sarkisov and Monson 2001; Cohan 1944). The cavity had a width of 4.34 nm and length of 10 nm. The isotherms are shown in Figs. 11 and 12, respectively.

The adsorption branch of the isotherm for the pore with the smaller neck shows two steps; the first corresponds to capillary condensation in the neck, and the second to growth of the adsorbed layer in the cavity, followed by condensation when the gas-like core is sufficiently small (delayed condensation) (Sarkisov and Monson 2001). On desorption from the filled pore, there is initially a gradual change in the adsorbate density as the meniscus recedes through the neck, followed by a steep decrease when adsorbate evaporates from the cavity. Further decrease in pressure then removes molecules from the remaining adsorbed layers.

When the neck size is increased from 3 to 3.67 nm, the two-stage condensation observed earlier, when the sizes of the cavity and the neck are different becomes a one-stage condensation because the sizes of the neck and the cavity are now very similar. The mechanism of adsorption and condensation in this pore is very similar to that in the closed end pore discussed in Sect. 3.2; that is after some layers have been built up on the pore walls, adsorption proceeds via the movement of a meniscus from the closed end towards the pore mouth. Upon desorption from a completely filled pore, the process is reversed, but is delayed because of the metastability of the liquid

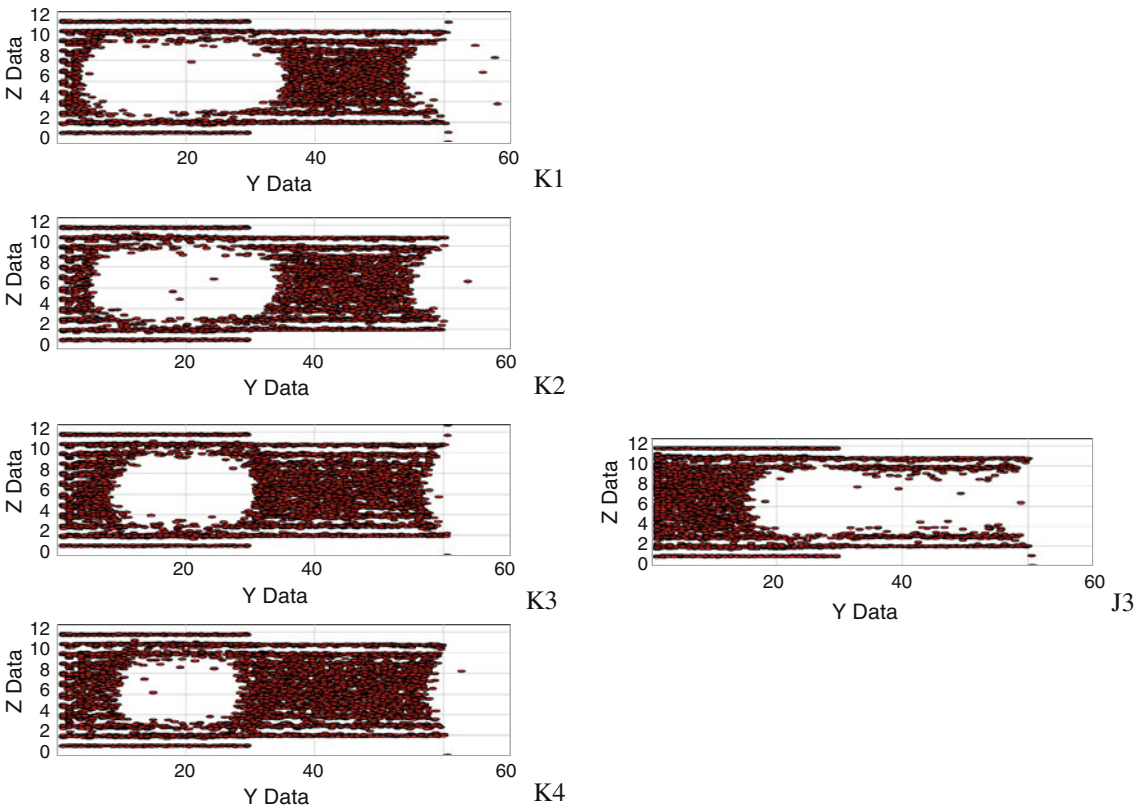


**Fig. 15** Snapshots of argon at 87.3 K at points K1–K4 in Fig. 12 through the equilibrium phase transition; determined from the Mid-Density scheme

condensate. The snapshots in Fig. 12 illustrate the molecular configurations at various stages in the adsorption desorption process.

### *3.4.2 Cavitation*

When the neck is smaller than the critical size the evaporation proceeds via a cavitation mechanism. Figure 13 shows the adsorption isotherm for an ink-bottle pore with cavity width 4.34 nm and neck width 2.33 nm. The lengths of the cavity and the neck are each 10 nm. There are two distinct hysteresis loops, associated with the neck and the cavity respectively. Adsorption begins with molecular layering on the pore walls, followed by condensation in the neck, corresponding to the first step in the adsorption branch. Once the neck has been completely filled, adsorption proceeds by movement of the two menisci in the cavity; one from the closed end and the other from the junction between the filled neck and the cavity. When the gas-like core in the cavity is small enough, condensation occurs, giving the second step in the adsorption branch. Desorption occurs in two stages, the first is due to the cavitation resulting from the stretching of the fluid beyond its stability limit, and the second is due to the two receding menisci in the neck, which behaves as a uniform pore with two open ends. Since the cavitation pressure in the cavity is greater than the evaporation pressure in the neck, the desorption branch proceeds in two stages.

The snapshots in Fig. 13 show the cavitation process at different stages of adsorption and desorption. It is interesting to note the changes in the size of the bubble just after the cavitation (P3), where metastability creates a large bubble over a small pressure interval, and filling of the gas-like core during condensation in the cavity (O3, O4, O5), which is much more gradual.

The effects of neck length on desorption, when cavitation occurs, is illustrated in Fig. 14. When the neck length was reduced to 2 nm (see plot 1, square with solid line), the capillary condensation shifts to a higher pressure. The adsorption branch associated with the cavity was unchanged because the cavity dimensions remain the same. However, when the length of the neck was changed from 10 to 2 nm for a pore model with a cavitation-controlled desorption branch (see Fig. 13), the evaporation pressure occurs at the same value (about 18 kPa, in this case). When the length of the neck was further reduced to 0.5 nm (plot 2, gray circle with solid line in Fig. 14), the hysteresis associated with the neck vanishes because the neck has negligible capacity compared to the cavity. The adsorbed amount on the desorption-branch before evaporation

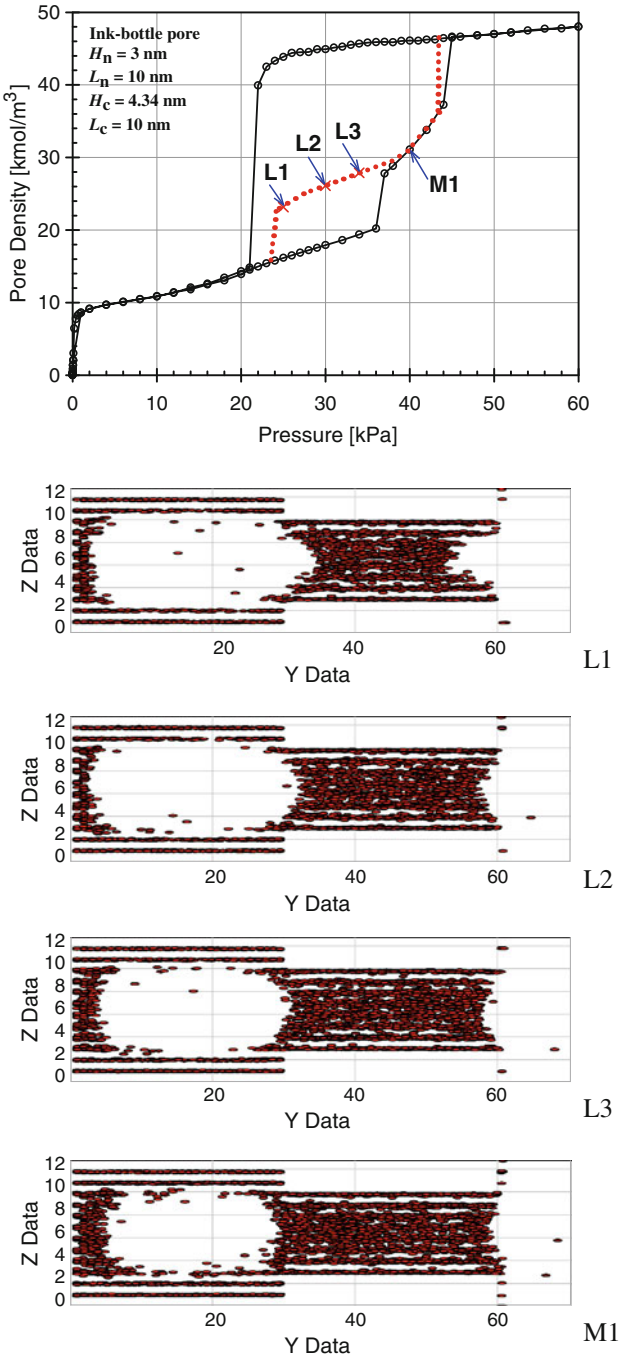


**Fig. 16** Snapshots of argon at 87.3 K showing the course of the equilibrium transition state; calculated using the Mid-Density scheme

changes slightly as the loss of mass is due to stretching of the fluid in the cavity. Evaporation occurs at a much higher pressure than in the pore with a longer neck. This sharp evaporation is described as cavitation-like pore blocking (Nguyen 2013), which depends on the pore geometry. The process differs from cavitation, which is a fluid property alone (Thommes et al. 2006), unless the cavity is small enough to stabilize the condensed fluid.

Plot 3 in the panel of Fig. 14 adds further evidence to this conclusion. Here, adsorption takes place in two stages; the first is due to condensation in the neck, and the second is associated with the cavity. Desorption occurs in a single stage with a small shoulder, because cavitation is followed almost immediately by evaporation from the neck; as shown by the snapshots S1 and S2 in Fig. 14. The cavitation pressure is slightly lower than that for the wider cavity.

### *3.4.3 Equilibrium transition*

The equilibrium transitions associated with the neck are close to the desorption branch, and similar to those in independent pores having the same width and open at both ends. On the other hand, the equilibrium transitions associated with the cavity are close to the adsorption-branch, and similar to those for a single pore with closed end discussed in Sect. 3.2.

The snapshots for the stable equilibrium transition are shown in Fig. 15. At points through the equilibrium transition a bubble appears in the cavity and remains stable because the neck is full. The penalty for the appearance of new interfaces (inside the bubble) is paid by the lower energy of the dense fluid in the neck. As pressure is reduced the two menisci move into the interior of the neck, as in the independent pore with two open ends. The stabilization of the bubble by the full neck is also seen in the equilibrium transition connecting two equilibrium transitions associated with the neck and the cavity, as illustrated in the snapshots of Fig. 16.

The equilibrium transitions in the pore where cavitation is the evaporation mechanism are shown as a dotted line in Fig. 13, and the corresponding snapshots in Fig. 17. The equilibrium states for the pore with cavitation are similar those in which blocking is the mechanism, suggesting that equilibrium is achieved when a bubble is formed and molecules can be relocated in positions where the solid–fluid and fluid–fluid interactions, which provide the stabilization force for maintaining the interfaces of the bubble, are maximised.

## 4 Conclusions

We have investigated the pore blocking and cavitation mechanisms in desorption from slit-shaped ink-bottle pores using Bin-GCMC simulation. These mechanisms are primarily dictated by the pore width of the neck, and are somewhat insensitive to neck length. When the neck width is less than some critical value, cavitation occurs; above this size, pore evaporation is by pore blocking. The two mechanisms can be distinguished by different forms of the

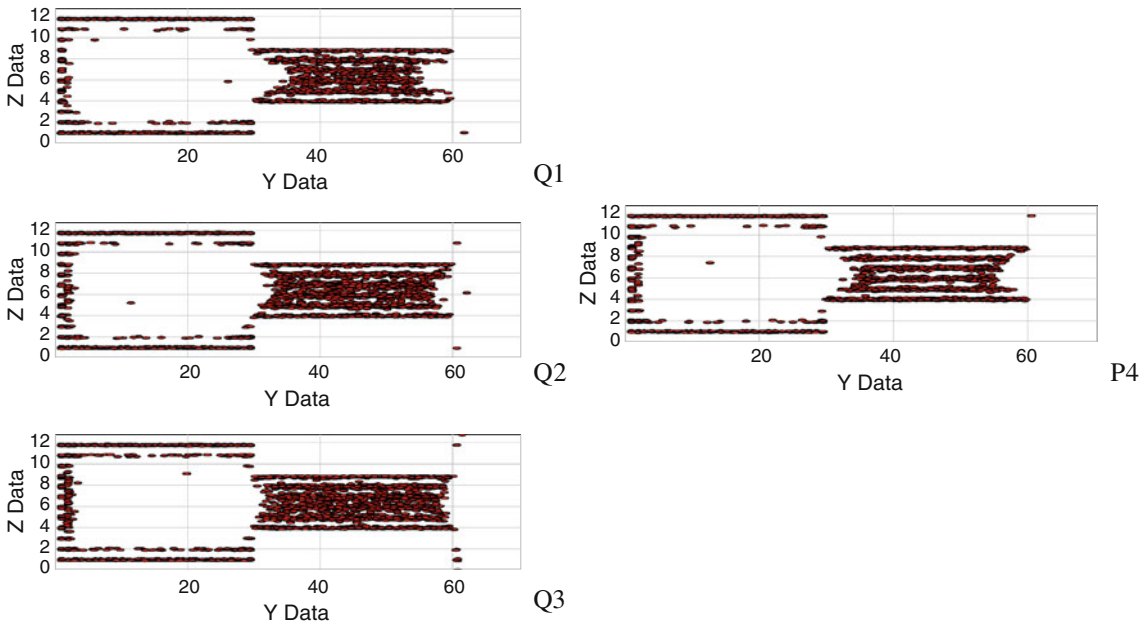


**Fig. 17** Snapshots of argon at 87.3 K, at points Q1–Q3 in Fig. 13, in the equilibrium transition; calculated by the Mid-Density scheme

desorption isotherm. When cavitation is the controlling mechanism, the desorption-branch decreases only gradually before a steep evaporation step. When pore blocking is the controlling mechanism, the initial decrease is steeper and there is a knee prior to evaporation.

The equilibrium transition in various ink-bottle pores has been determined using the recently developed Mid-Density scheme, and has three stages: the first is associated with the neck and is close to the desorption branch, the third is associated with the cavity and is close to the adsorption branch, whilst the second stage, joining the other two stages, falls between the adsorption and desorption branches.

By changing the neck length in our cavitation models, we have been able to show that the pressure at which a pore empties on desorption is dependent on pore geometry, and not simply on the fluid properties alone.

**Acknowledgments** This research was made possible by the Australian Research Council and Suranaree University of Technology whose support are gratefully acknowledged. We also acknowledge the support from the Office of the Commission on Higher Education of Thailand in the form of Ph.D. scholarship to NK.

## Appendix

The interaction of a particle and a strip which is finite in one direction ($y$-direction) and infinite in the other ($x$-direction) (shown in Fig. 18) is calculated from the Bojan–Steele equation (Bojan and Steele 1988, 1989, 1993):

$$U_{i,s} = \sum_{a=1}^{M} 2\pi\varepsilon_i^{a,s}\rho_s(\sigma_i^{a,s})^2 \cdot \times\left\{\left[U_{rep}(y_i^{a,+}, z_i^a) - U_{rep}(y_i^{a,-}, z_i^a)\right] - \left[U_{att}(y_i^{a,+}, z_i^a) - U_{att}(y_i^{a,-}, z_i^a)\right]\right\} \quad (6)$$

where

$$y_i^{a,+} = \frac{L}{2} - y_i^a; \quad y_i^{a,-} = -\frac{L}{2} - y_i^a \quad (7)$$

The repulsive and attractive terms on the right hand side of Eq. (6) are given by:

$$U_{\text{rep}}(y,z) = \frac{y}{\sqrt{y^2+z^2}}\left\{\frac{1}{5}\left(\frac{\sigma_i^{a,s}}{z}\right)^{10} + \frac{1}{10}\frac{(\sigma_i^{a,s})^{10}}{z^8(y^2+z^2)} + \frac{3}{40}\frac{(\sigma_i^{a,s})^{10}}{z^6(y^2+z^2)^2} + \frac{1}{16}\frac{(\sigma_i^{a,s})^{10}}{z^4(y^2+z^2)^3} + \frac{7}{128}\frac{(\sigma_i^{a,s})^{10}}{z^2(y^2+z^2)^4}\right\} \quad (8)$$

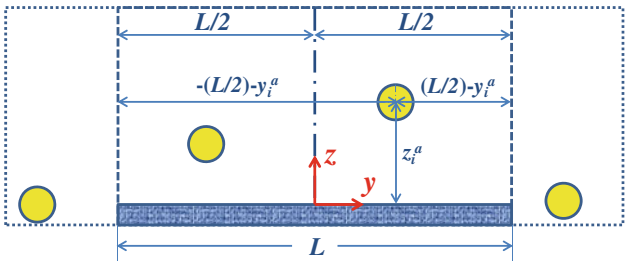


**Fig. 18** Configuration of a finite strip

$$U_{\mathrm{att}}(y,z)=\frac{y}{\sqrt{y^2+z^2}}\left\{\frac{1}{2}\left(\frac{\sigma_i^{a,s}}{z}\right)^4+\frac{1}{4}\frac{(\sigma_i^{a,s})^4}{z^2(y^2+z^2)}\right\} \tag{9}$$

where $z_i^a$ is the distance of site $a$ of molecule $i$ from the graphite surface, $\varepsilon_i^{a,s}$ and $\sigma_i^{a,s}$are the adsorptive-graphite interaction potential well-depth and intermolecular collision diameter respectively, and $\rho_s$ is the surface density (taken as 38.2 $\mathrm{nm}^{-2}$ in this study). The cross parameters, $\sigma_i^{a,s}$and $\varepsilon_i^{a,s}$can be determined by the Lorentz–Berthelot mixing rules: $\sigma_i^{a,s}=(\sigma_i^{a,a}+\sigma^s)/2$ and $\varepsilon_i^{a,s}=(\varepsilon_i^{a,a}\varepsilon^s)^{1/2}$ where the parameters for a carbon atom in a graphene layer are $\sigma^s=0.34$ nm and $\varepsilon^s/k_B=28.0$ K.The potential equation energy in Eqs. (6)–(9) is valid for any positions around the strip, except $z_i^a\rightarrow 0$, and in such cases we use the following Taylor series expansion:

$$\begin{aligned}\frac{U_{i,s}}{2\pi K\rho_s}=\sum_{a=1}^{M}\varepsilon_i^{a,s}(\sigma_i^{a,s})^2\Bigg(&\left\{\frac{63}{1280}\left[\left(\frac{\sigma_i^{a,s}}{y_i^{a,-}}\right)^{10}-\left(\frac{\sigma_i^{a,s}}{y_i^{a,+}}\right)^{10}\right]\right.\\&\left.-\frac{3}{16}\left[\left(\frac{\sigma_i^{a,s}}{y_i^{a,-}}\right)^{4}-\left(\frac{\sigma_i^{a,s}}{y_i^{a,+}}\right)^{4}\right]\right\}\\&-\left(\frac{z_i^a}{\sigma_i^{a,s}}\right)^2\left\{\frac{231}{1024}\left[\left(\frac{\sigma_i^{a,s}}{y_i^{a,-}}\right)^{12}-\left(\frac{\sigma_i^{a,s}}{y_i^{a,+}}\right)^{12}\right]\right.\\&\left.-\frac{5}{16}\left[\left(\frac{\sigma_i^{a,s}}{y_i^{a,-}}\right)^{6}-\left(\frac{\sigma_i^{a,s}}{y_i^{a,+}}\right)^{6}\right]\right\}\\&+\left(\frac{z_i^a}{\sigma_i^{a,s}}\right)^4\left\{\frac{1287}{2048}\left[\left(\frac{\sigma_i^{a,s}}{y_i^{a,-}}\right)^{14}-\left(\frac{\sigma_i^{a,s}}{y_i^{a,+}}\right)^{14}\right]\right.\\&\left.-\frac{105}{256}\left[\left(\frac{\sigma_i^{a,s}}{y_i^{a,-}}\right)^{8}-\left(\frac{\sigma_i^{a,s}}{y_i^{a,+}}\right)^{8}\right]\right\}\\&-\left(\frac{z_i^a}{\sigma_i^{a,s}}\right)^6\left\{\frac{45045}{32768}\left[\left(\frac{\sigma_i^{a,s}}{y_i^{a,-}}\right)^{16}-\left(\frac{\sigma_i^{a,s}}{y_i^{a,+}}\right)^{16}\right]\right.\\&\left.-\frac{63}{128}\left[\left(\frac{\sigma_i^{a,s}}{y_i^{a,-}}\right)^{10}-\left(\frac{\sigma_i^{a,s}}{y_i^{a,+}}\right)^{10}\right]\right\}\\&+\left(\frac{z_i^a}{\sigma_i^{a,s}}\right)^8\left\{\frac{85085}{32768}\left[\left(\frac{\sigma_i^{a,s}}{y_i^{a,-}}\right)^{18}-\left(\frac{\sigma_i^{a,s}}{y_i^{a,+}}\right)^{18}\right]\right.\\&\left.-\frac{1155}{2048}\left[\left(\frac{\sigma_i^{a,s}}{y_i^{a,-}}\right)^{12}-\left(\frac{\sigma_i^{a,s}}{y_i^{a,+}}\right)^{12}\right]\right\}+O(z/\sigma_i^{a,s})^{10}\Bigg)\end{aligned} \tag{10}$$

where $K=1$ for positive values of $y_i^{a,+}$and $y_i^{a,-}$, $K=-1$ for negative values of $y_i^{a,+}$ and $y_i^{a,-}$.

## References


Allen, M.P., Tildesley, T.P.: Computer Simulation of Liquids. Clarendon, Oxford (1987)

Bojan, M.J., Steele, W.A.: Computer simulation of physisorption on a heterogeneous surface. Surf. Sci. **199**, L395–L402 (1988)

Bojan, M.J., Steele, W.A.: Computer-simulation of physisorbed Kr on a heterogeneous surface. Langmuir **5**, 625–633 (1989)

Bojan, M.J., Steele, W.A.: Computer-simulation of physical adsorption on stepped surfaces. Langmuir **9**, 2569–2575 (1993)

Cohan, L.H.: Hysteresis and the capillary theory of adsorption of vapors. J. Am. Chem. Soc. **66**, 98–105 (1944)

Do, D.D., Do, H.D.: Effects of potential models in the vapor-liquid equilibria and adsorption of simple gases on graphitized thermal carbon black. Fluid Phase Equilib. **236**, 169–177 (2005)

Do, D.D., Herrera, L.F., Do, H.D.: A new method to determine pore size and its volume distribution of porous solids having known atomistic configuration. J. Colloid and Interface Sci. **328**, 110–119 (2008)

Edison, J.R., Monson, P.A.: Dynamic mean field theory of condensation and evaporation in model pore networks with variations in pore size. Microporous Mesoporous Mater. **154**, 7–15 (2012)

Fan, C.Y., Do, D.D., Nicholson, D.: On the cavitation and pore blocking in slit-shaped ink-bottle pores. Langmuir **27**, 3511–3526 (2011a)

Fan, C.Y., Do, D.D., Nicholson, D.: New Monte Carlo simulation of adsorption of gases on surfaces and in pores: a concept of multibins. J. Phys. Chem. B **115**, 10509–10517 (2011b)

Fan, C.Y., Razak, M.A., Do, D.D., Nicholson, D.: On the Identification of the sharp spike in the heat curve for argon, nitrogen, and methane adsorption on graphite: reconciliation between computer simulation and experiments. J. Phys. Chem. C **116**, 953–962 (2012)

Grant, S.M., Jaroniec, M.: Effect of cosolvent organic molecules on the adsorption and structural properties of soft-templated ordered mesoporous alumina. J. Colloid Interface Sci. **367**, 129–134 (2012)

Grosman, A., Ortega, C.: Capillary condensation in porous materials—hysteresis and interaction mechanism without pore blocking/percolation process. Langmuir **24**, 3977–3986 (2008)

Grosman, A., Ortega, C.: Cavitation in metastable fluids confined to linear mesopores. Langmuir **27**, 2364–2374 (2011)

Hauschild, T., Prausnitz, J.M.: Monte-Carlo calculations for methane and argon over a wide-range of density and temperature, including the two-phase vapor-liquid region. Mol. Simul. **11**, 177–185 (1993)

Horikawa, T., Hayashi, J., Muroyama, K.: Controllability of pore characteristics of resorcinol-formaldehyde carbon aerogel. Carbon **42**, 1625–1633 (2004)

Horikawa, T., Do, D.D., Nicholson, D.: Capillary condensation of adsorbates in porous materials. Adv. Colloid Interface Sci. **169**, 40–58 (2011)

Jorge, M., Seaton, N.A.: Molecular simulation of phase coexistence in adsorption in porous solids. Mol. Phys. **100**, 3803–3815 (2002)

Kierlik, E., Monson, P.A., Rosinberg, M.L., Tarjus, G.: Adsorption hysteresis and capillary condensation in disordered porous solids: a density functional study. J. Phys.-Condens. Mater **14**, 9295–9315 (2002)

Klomkliang, N., Do, D.D., Nicholson, D.: On the hysteresis and equilibrium phase transition of argon and benzene adsorption in finite slit pores: Monte Carlo vs Bin-Monte Carlo. Chem. Eng. Sci. **87**, 327–337 (2013)

Kruk, M., Jaroniec, M.: Argon adsorption at 77 K as a useful tool for the elucidation of pore connectivity in ordered materials with large cagelike mesopores. Chem. Mater. **15**, 2942–2949 (2003)

Libby, B., Monson, P.A.: Adsorption/desorption hysteresis in inkbottle pores: a density functional theory and Monte Carlo simulation study. Langmuir **20**, 4289–4294 (2004)

Liu, H., Zhang, L., Seaton, N.A.: Sorption hysteresis as a probe of pore structure. Langmuir **9**(10), 2576–2582 (1993)

Liu, J., Zhang, L., Yang, Q., Li, C.: Structural control of mesoporous silicas with large nanopores in a mild buffer solution. Microporous Mesoporous Mater. **116**, 330–338 (2008)

Liu, Z.J., Herrera, L., Nguyen, V.T., Do, D.D., Nicholson, D.: A Monte Carlo scheme based on Mid-Density in a hysteresis loop to determine equilibrium phase transition. Mol. Simul. **37**, 932–939 (2011)

Liu, Z.J., Do, D.D., Nicholson, D.: A thermodynamic study of the Mid-Density scheme to determine the equilibrium phase transition in cylindrical pores. Mol. Simul. **38**, 189–199 (2012)

Lu, A.H., Schüth, F.: Nanocasting pathways to create ordered mesoporous solids. C. R. Chim. **8**, 609–620 (2005)

Lu, A.H., Schüth, F.: Nanocasting: a versatile strategy for creating nanostructured porous materials. Adv. Mater. **18**, 1793–1805 (2006)

Mason, G.: A model of adsorption–desorption hysteresis in which hysteresis is primarily developed by the interconnections in a network of pores. Proceedings of the Royal Society of London. A. Mathematical and Physical Sciences, **390**: p. 47-72 (1983)

Mayagoitia, V., Rojas, F., Kornhauser, I., Pérez-Aguilar, H.: Modeling of porous media and surface structures: their true essence as networks. Langmuir **13**, 1327–1331 (1997)

McBain, J.W.: An explanation of hysteresis in the hydration and dehydration of gels. J. Am. Chem. Soc. **57**, 699–700 (1935)

Morishige, K.: Adsorption hysteresis in ordered mesoporous silicas. Adsorpt.-J. Int. Adsorpt. Soc. **14**, 157–163 (2008)

Morishige, K., Ito, M.: Capillary condensation of nitrogen in MCM-41 and SBA-15. J. Chem. Phys. **117**, 8036–8041 (2002)

Morishige, K., Tateishi, N.: Adsorption hysteresis in ink-bottle pore. J. Chem. Phys. **119**, 2301–2306 (2003)

Morishige, K., Yasuki, T.: Large-pore cagelike silica with necks of molecular dimensions. J. Phys. Chem. C **114**, 10910–10916 (2010)

Morishige, K., Yoshida, K.: Neck size of ordered cage-type mesoporous silica FDU-12 and origin of gradual desorption. J. Phys. Chem. C **114**, 7095–7101 (2010)

Morishige, K., Tateishi, N., Fukuma, S.: Capillary condensation of nitrogen in MCM-48 and SBA-16. J. Phys. Chem. B **107**, 5177–5181 (2003)

Morishige, K., Tateishi, M., Hirose, F., Aramaki, K.: Change in desorption mechanism from pore blocking to cavitation with temperature for nitrogen in ordered silica with cagelike pores. Langmuir **22**, 9220–9224 (2006)

Neimark, A.V., Vishnyakov, A.: Gauge cell method for simulation studies of phase transitions in confined systems. Phys. Rev. E **62**, 4611–4622 (2000)

Neimark, A.V., Ravikovitch, P.I., Vishnyakov, A.: Bridging scales from molecular simulations to classical thermodynamics: density functional theory of capillary condensation in nanopores. J. Phys.-Condens Matter **15**, 347–365 (2003)

Nguyen, P.T.M., Do, D.D., Nicholson, D.: On the cavitation and pore blocking in cylindrical pores with simple connectivity. J. Phys. Chem. B **115**, 12160–12172 (2011)

Nguyen, P., Fan, C., Do, D.D., Nicholson, D.: On the cavitation-like pore blocking in ink-bottle pore. J. Phys. Chem. C **117**, 5475 (2013)

Nicholson, D.: Capillary models for porous media—part 2: sorption desorption hysteresis in three dimensional networks. Trans. Faraday Soc. **64**, 3416–3424 (1968)

Peterson, B.K., Gubbins, K.E.: Phase transitions in a cylindrical pore: grand canonical Monte-Carlo, mean field-theory and the Kelvin equation. Mol. Phys. **62**, 215–226 (1987)

Peterson, B.K., Gubbins, K.E., Heffelfinger, G.S., Marconi, U.M.B., Vanswol, F.: Lennard-Jones fluids in cylindrical pores: nonlocal theory and computer-simulation. J. Chem. Phys. **88**, 6487–6500 (1988)

Puibasset, J.: Counting metastable states within the adsorption/desorption hysteresis loop: a molecular simulation study of confinement in heterogeneous pores. J. Chem. Phys. **133**, 104701–104714 (2010)

Rasmussen, C.J., Vishnyakov, A., Thommes, M., Smarsly, B.M., Kleitz, F., Neimark, A.V.: Cavitation in metastable liquid nitrogen confined to nanoscale pores. Langmuir **26**, 10147–10157 (2010)

Rasmussen, C.J., Gor, G.Y., Neimark, A.V.: Monte Carlo simulation of cavitation in pores with nonwetting defects. Langmuir **28**, 4702–4711 (2012)

Ravikovitch, P.I., Neimark, A.V.: Experimental confirmation of different mechanisms of evaporation from ink-bottle type pores: equilibrium, pore blocking, and cavitation. Langmuir **18**, 9830–9837 (2002)

Reichenbach, C., Kalies, G., Enke, D., Klank, D.: Cavitation and pore blocking in nanoporous glasses. Langmuir **27**, 10699–10704 (2011)

Rigby, S.P., Fletcher, R.S.: Experimental evidence for pore blocking as the mechanism for nitrogen sorption hysteresis in a mesoporous material. J. Phys. Chem. B **108**, 4690–4695 (2004)

Rowley, L.A., Nicholson, D., Parsonage, N.G.: Monte-Carlo grand canonical ensemble calculation in a gas-liquid transition region for 12-6 argon. J. Comput. Phys. **17**, 401–414 (1975)

Sahu, D.R., Hong, L.Y., Wang, S.C., Huang, J.L.: Synthesis, analysis and characterization of ordered mesoporous TiO2/SBA-15 matrix: effect of calcination temperature. Microporous Mesoporous Mater. **117**, 640–649 (2009)

Sarkisov, L., Monson, P.A.: Modeling of adsorption and desorption in pores of simple geometry using molecular dynamics. Langmuir **17**, 7600–7604 (2001)

Sing, K.S.W., Everett, D.H., Haul, R.A.W., Moscou, L., Pierotti, R.A., Rouquerol, J., Siemieniewska, T.: Reporting physisorption data for gas/solid systems with special reference to the determination of surface area and porosity (Recommendations 1984). Pure Appl. Chem. **57**, 603–619 (1985)

Steele, W.A.: Physical interaction of gases with crystalline solids—1 Gas-solid energies and properties of isolated adsorbed atoms. Surf. Sci. **36**, 317–352 (1973)

Thommes, M., Smarsly, B., Groenewolt, M., Ravikovitch, P.I., Niemark, A.V.: Adsorption hysteresis of nitrogen and argon in pore networks and characterization of novel micro- and mesoporous silicas. Langmuir **22**, 756–764 (2006)

Vishnyakov, A., Neimark, A.V.: Studies of liquid-vapor equilibria, criticality, and spinodal transitions in nanopores by the gauge cell Monte Carlo simulation method. J. Phys. Chem. B **105**, 7009–7020 (2001)

Vishnyakov, A., Neimark, A.V.: Monte Carlo simulation test of pore blocking effects. Langmuir **19**, 3240–3247 (2003a)

Vishnyakov, A., Neimark, A.V.: Nucleation of liquid bridges and bubbles in nanoscale capillaries. J. Chem. Phys. **119**, 9755–9764 (2003b)